Journal of Power Sources 196 (2011) 6815–6821

Contents lists available at ScienceDirect

Journal of Power Sources

journal homepage: www.elsevier.com/locate/jpowsour

TiO_2 rutile—An alternative anode material for safe lithium-ion batteries

M. Pfanzelt, P. Kubiak*, M. Fleischhammer, M. Wohlfahrt-Mehrens

ZSW-Zentrum für Sonnenenergie- und Wasserstoff- Forschung, Helmholtzstrasse 8, D-89081 Ulm, Germany

ARTICLE INFO

Article history:
Received 12 August 2010
Received in revised form
20 September 2010
Accepted 29 September 2010
Available online 14 October 2010

Keywords:
TiO_2 rutile
Lithium-ion batteries
Impedance spectroscopy
Thermal analysis

ABSTRACT

We investigate the properties of nanosized TiO_2 rutile by electrochemical methods and thermal analysis. The material shows a high capacity, high rate performance and excellent cycling stability. We can clearly prove the safer character of rutile electrodes by thermal analysis. The lithiated rutile electrodes exhibit exothermic reactions with a very small energy release and they are mainly related to surface film (SEI) decomposition. The impedance spectra strongly indicate the formation of a surface film, but the semicircles of charge transfer and SEI formation cannot be resolved at any potential. In addition a new pouch cell design which is suitable for in situ measurements such as FTIR, Raman and XRD is introduced and its efficiency is proven by in situ optical microscopy.

1. Introduction

Lithium-ion batteries are the major electrochemical power sources in the field of non stationary applications. But to meet the future demands of the market in the fields of hybrid electric vehicles (HEV) and electric vehicles (EV), further improvements are necessary, especially in terms of cost reduction, higher power and energy densities, long life time and safety [1–3]. Graphite as a standard anode material presents a poor cycling behaviour at high rates as well as at low temperatures [4], a high irreversible capacity in the first cycle due to the solid electrolyte interface (SEI) formation [5] and safety issues in the charged (lithiated) state [6–9]. Hence alternative anode materials with a better cycling ability and safety are needed. TiO_2 materials have become an interesting anode material for lithium-ion batteries with unique properties such as high power densities, cheapness, safety and non-toxicity. Different polymorphs of TiO_2 (e.g. anatase, TiO_2 (B), brookite and rutile) have been investigated as possible lithium-ion insertion compounds [10–13]. Their theoretical capacity is 335 mA h g^{-1} corresponding to the insertion of 1 lithium per mol of TiO_2 according to the following equation:

$$TiO_2 + x(Li^+ + e^-) \leftrightarrows Li_xTiO_2 \text{ with } x = 1$$

Bulk rutile was investigated as a possible candidate for lithium-ion batteries for a long time, but only Macklin and Neat could demonstrate a successful Li^+ insertion and extraction at 120 °C in a lithium polymer cell [14]. From these observations, it was commonly believed that rutile can only insert/extract negligible amounts of Li^+ at room temperature. This picture totally changed in 2006 after the demonstration of the reversible Li^+ insertion/extraction of ~0.5 mol Li per mol TiO_2 at room temperature into/from nanosized rutile [15,16]. Kinetic limitations have been proposed to explain the difference between microsized and nanosized TiO_2 rutile [17,18]. Lithium insertion/extraction into/from rutile is highly anisotropic and proceeds mainly through fast diffusion along the *c*-axis channels while Li diffusion in the *ab*-planes is very slow. The theoretical Li^+ diffusion coefficients along the *c*-axis and the *ab*-plane are 10^{-6} cm^2 s^{-1} and 10^{-14} cm^2 s^{-1} respectively [19–22]. A practical determination of the diffusion coefficient is difficult due to the unknown active surface and may differ for each nanosized sample with different crystallite sizes and shapes. With a reversible accommodation of lithium into the rutile structure up to ~$Li_{0.55}TiO_2$ (~185 mA h g^{-1}) at 1–3 V vs. Li/Li^+ and ~$Li_{0.9}TiO_2$ (~300 mA h g^{-1}) at 0.1–3 V the capacity of nanosized rutile is competitive to graphite anodes [23].

In this study we investigated the behaviour of nanosized rutile in two potential windows 1–3 V and 0.1–3 V by galvanostatic and impedance measurements. To study the safety properties of TiO_2 rutile we compared the thermal behaviour of lithiated and delithiated rutile electrodes with standard graphite electrodes in the temperature range from 30 to 350 °C. In addition we present a new two electrode pouch cell with a lithium iron phosphate cathode and a rutile anode which is suitable for in situ measurements. Using this cell we obtained first results of an in situ optical microscopy experiment with a carbon free rutile electrode.

* Corresponding author. Tel.: +49 (0)7319530401; fax: +49 (0)7319530666.
E-mail address: pierre.kubiak@zsw-bw.de (P. Kubiak).

0378-7753/$ – see front matter © 2010 Elsevier B.V. All rights reserved.
doi:10.1016/j.jpowsour.2010.09.109

2. Experimental

2.1. Materials

The synthesis of nanosized rutile was already reported elsewhere [24]. Sodium dodecylsulfate (SDS, Merck) was dissolved in diluted hydrochloric acid (pH 0) and a glycerol modified TiO_2 precursor (bis(1,2,3-trihydroxypropyl)titanate, prepared from titanium isopropoxide and glycerol) was added. After ageing at 60 °C overnight, the resulting powder was centrifuged, washed with water, dried at 60 °C overnight and finally annealed at 400 °C for 4 h.

Lithium iron phosphate (P2 from Süd-Chemie) was used as cathode material for the in situ pouch cell. Graphite (active material: MAGD, Hitachi Chem., Japan) electrodes without conductive carbon were prepared for TG/DSC measurements.

2.2. Characterisation methods

X-ray diffraction measurements were performed using Cu-Kα radiation (λ = 0.154 nm) on a Siemens D5000 and the data was evaluated with the program TOPAS 2.1 from Bruker. Scanning Electron Microscopy (SEM) pictures were taken on a LEO 1530 VP. Transmission Electron Microscopy (TEM) was performed on a Titan 80–300 kV. In this study we used a NETSZCH STA 449C Jupiter for the Thermogravimetry (TG) and Differential Scanning Calorimetry (DSC) at a scan rate of 10 °C min^{-1} in the temperature range of 30–350 °C, under argon flux. To analyse the produced gases a mass spectrometer (MS) (NETSZCH QMS 403C electron impact, channeltron, 1.4 kV Aëolos) was coupled with the above described TG/DSC instrument. The lithiated/delithiated electrodes were analysed directly after cycling (lithiated electrodes 2.5 cycles, delithiated electrodes 3 cycles).

2.3. Electrode preparation and electrochemical evaluation

The anode electrodes were manufactured by mixing TiO_2:carbon black (Timcal, Super P):polyvinylidene fluoride in the ratio 76:12:12 wt%. Afterwards a few mL N-Methylpyrrolidone (NMP) were added to coat the resulting slurry on a cupper foil using "doctor blade" technique (thickness 150 μm). The electrode film was dried at 40 °C for 1 h and then punched into circular disks with a mass loading of ~2 mg cm^{-2}. After that the electrode disks were pressed, dried under vacuum and transferred in an argon filled glovebox (MBRAUN) with a water and oxygen content less than 1 ppm. For galvanostatic and impedance measurements a three electrode cell was used with lithium as counter and reference electrode, TiO_2 as working electrode, glass microfiber (Whatman, GF/A) as separator and 1 M $LiPF_6$ in EC:DMC (1:1 wt%) (UBE Industry, Japan) as electrolyte.

All the measurements were carried out at room temperature using a VMP/Z (Princeton, Biologic) electrochemical workstation for galvanostatic and impedance measurements. The frequency range of the impedance measurements was 0.01–75,000 Hz and the evaluation of the received data was done with the program Boukamp [25,26]. A χ^2 value $<10^{-3}$ indicates a good agreement between simulated spectra and recorded data. All potentials mentioned in this study are given vs. Li/Li^+. For all electrochemical measurements the maximum x in Li_xTiO_2 is assumed to be 1 (335 mA h g^{-1}) and thus, all charging rates were based on TiO_2 according to the following relationship: 1 C = 0.335 A g^{-1}.

2.4. Pouch cell for in situ optical microscopy measurements

A special pouch cell with a $LiFePO_4$ cathode, a TiO_2 anode and a Celgard® separator was used for the in situ microscopy measurement. In order to have a free view directly onto the rutile anode, a circular disk was cut into the cathode and the separator (Fig. 1a and b). The components were placed into a transparent plastic bag, electrolyte was added and the whole pouch cell was sealed in an argon filled glovebox.

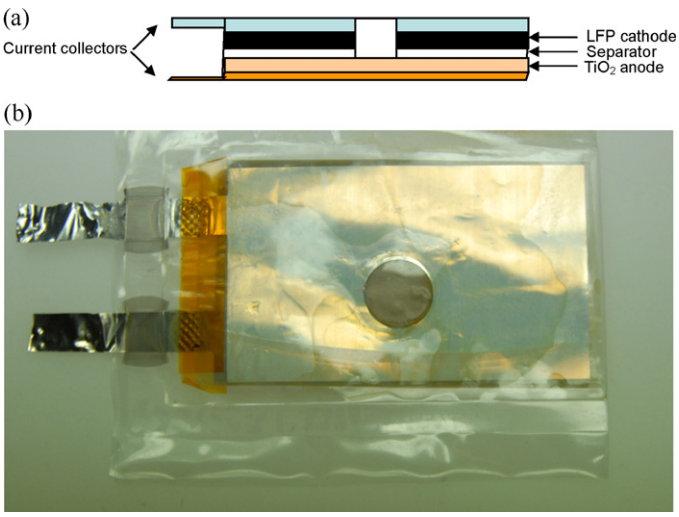

Fig. 1. Scheme of the pouch cell for in situ measurements (a) with a lithium iron phosphate cathode and a TiO_2 rutile anode. (b) Image of the pouch cell with a direct view onto the anode side (brown). (For interpretation of the references to color in this figure legend, the reader is referred to the web version of this article.)

3. Results and discussion

3.1. Material characterisation

The X-ray diffraction (XRD) patterns of the synthesised sample are shown in Fig. 2. All reflexes were assigned to TiO_2 rutile (JCPDS 21-1276 a = 4.593 Å; c = 2.959 Å) and they are broadened due to the low crystallite size. The refinement made by TOPAS (Total Pattern Analysis from Bruker) converges to the measured data and the lattice parameters of the space group $P4_2/mnm$ were calculated to a = 4.592 Å and c = 2.959 Å which is in good agreement with the reference values. The shape of the crystallites detected by TEM (Fig. 3a) is whisker-like with a diameter in the ab-plane of 5–6 nm and a length of ~50 nm in the c-direction. The whiskers are ordered in a ball-like and a parallel arrangement which is consistent with the SEM pictures (Fig. 3b).

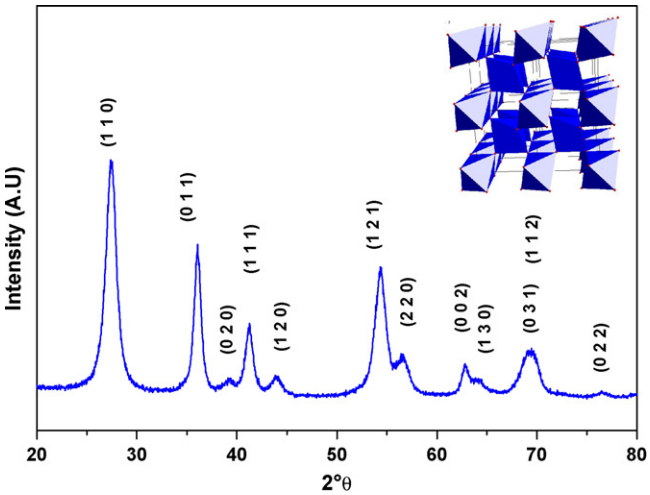

Fig. 2. XRD of the investigated TiO_2 sample after calcination. All reflexes can be assigned to rutile.

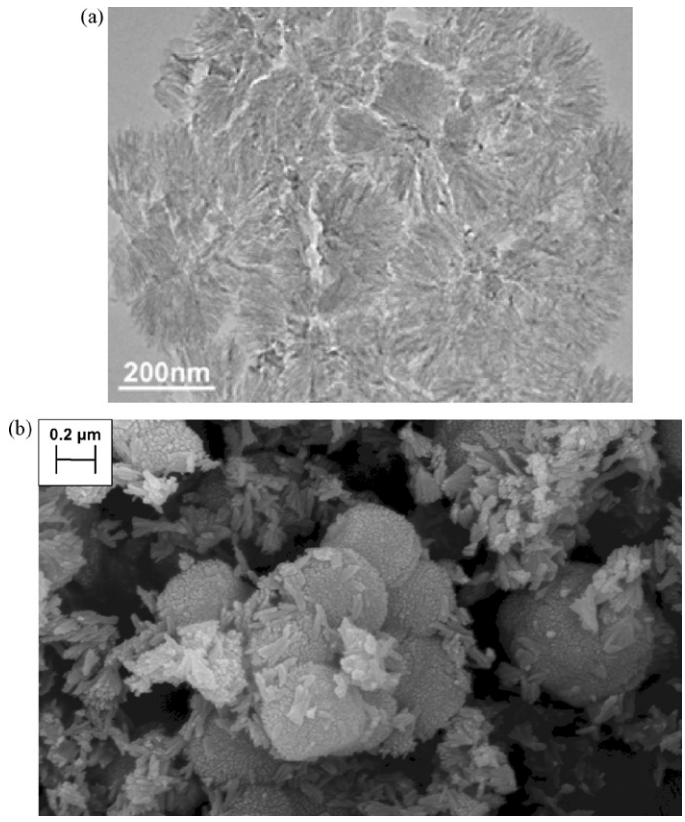

Fig. 3. Transmission electron microscopy pictures of the annealed rutile sample (a) and scanning microscopy image (b).

In our previous paper we have reported electrochemical results of this nanosized rutile sample [23]. The material combines excellent capacity values for charge/discharge rates from C/5 up to 5 C. An enlargement of the potential limits to 0.1–3 V results in a higher capacity for charging rates ranging from C/5 to 5 C (Fig. 4a). In order to investigate the cycling stability we performed 1000 cycles at 5 C in the potential range of 1–3 V with the first 5 cycles C/5 to achieve stable cycling conditions (Fig. 4b). We observed a constant cycling behaviour with an end capacity of 105 mA h g^{-1} after 1000 cycles which is ~70% of the initial capacity.

Electrochemical investigations during the first discharge of nanosized rutile revealed two dominating plateaus at 1.4 and 1.1 V vs. Li/Li^+ respectively corresponding to 2 two-phase mechanisms and afterwards a slope like decay down to 0.1 V. The first galvanostatic cycle is characterised by a huge irreversible capacity loss which increases with increasing potential range (Fig. 5). Therefore, in our previous communication we suggested the formation of a SEI-like film especially at potential below 0.8 V vs. Li/Li^+ [23]. To investigate the influence of this surface film on the material properties we performed TG/DSC and impedance measurements.

3.2. TG/DSC measurements

TG/DSC with an analysis of the produced gases by MS provides useful information about the thermal stability and the safety of a battery material. The preparation of lithiated and delithiated samples was carried out by galvanostatic cycling. The comparison between the graphite system and rutile in the charged and discharged state is shown in Fig. 6a and b and the detailed data are given in Table 2. The fully lithiated graphite (Fig. 6a) presented an exothermic peak $A_{Gr.}$ which is assigned to SEI decomposition and two peaks $B_{Gr.}'$ and $B_{Gr.}''$ with a large ΔH value (202.5 mW mg^{-1}). In the literature, the exothermic heat generation of graphite anodes is mainly attributed to reactions of the SEI. Although the exact reaction mechanism is still under discussion, one possibility is that the first exothermic peak is related to the SEI decomposition to form a secondary SEI and the subsequent ones are related to a breakdown of the secondary SEI followed by an exothermic reaction between the electrolyte and the intercalated lithium [6–9]. Up to now there have not been any studies about the thermal behaviour of rutile electrodes. The lithiated rutile sample showed only two exothermic peaks ($A_{Rt.}$ and $B_{Rt.}$) with low ΔH values (18.3 and 3.0 J g^{-1}) in comparison to graphite. Peak $A_{Rt.}$ had a similar onset temperature and shape in comparison to the graphite peak $A_{Gr.}$ while peak $B_{Rt.}$ was not present in the graphite curve. Both peaks $A_{Rt.}$ and $B_{Rt.}$ evoked typical electrolyte fragments in the mass spectrometer.

Delithiated samples of graphite and rutile were also prepared and analysed (Fig. 6b). The exothermic peak $A_{Gr.}$ of the graphite electrode can again be attributed to the SEI decomposition. The peaks $B_{Gr.}'$ and $B_{Gr.}''$ disappeared due to the missing intercalated lithium and an endothermic peak $C_{Gr.}$ showed up which was associated to a huge mass loss. Additionally the mass spectrometer detected typical electrolyte fragments for C_{Gr}. Therefore the only possible reaction corresponding to this peak was the electrolyte evaporation. The DSC curve of the delithiated rutile electrode showed similar shape with an exothermic peak $A_{Rt.}$ and an endothermic peak B_{Rt}. As the shape and onset temperature of $A_{Rt.}$ in the lithiated and the delithiated state was comparable to the

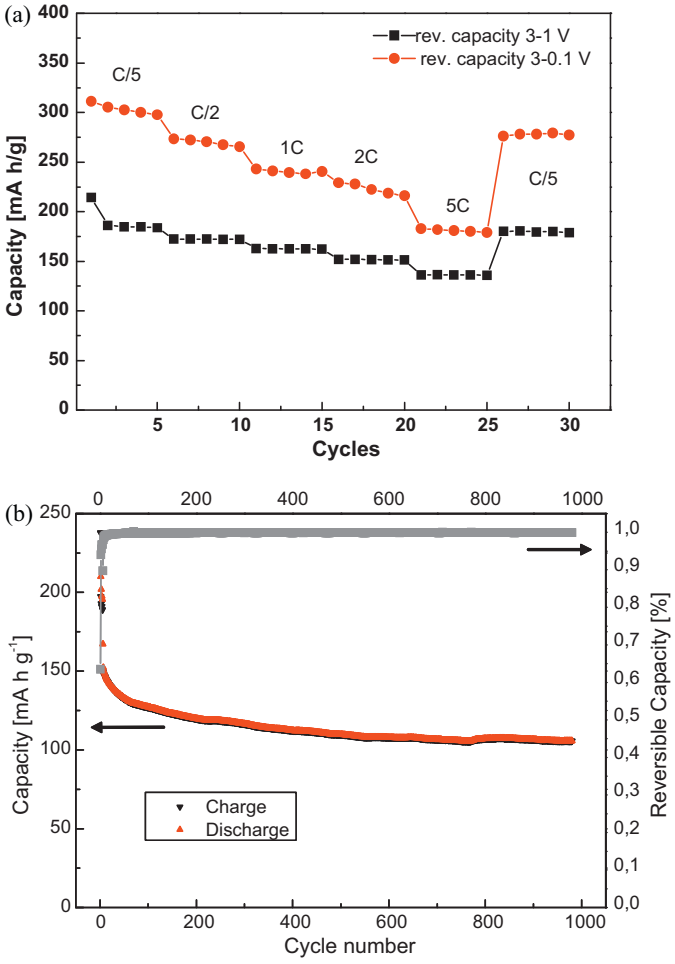

Fig. 4. Evolution of the reversible capacity from C/5 to 5 C in the potential window of 1–3 V (■) and 0.1–3 (●) (a). Cycling stability and coulombic efficiency of 1000 cycles at a charging rate of 5 C (b) (first 5 cycles at C/5). (For interpretation of the references to color in this figure legend, the reader is referred to the web version of this article.)

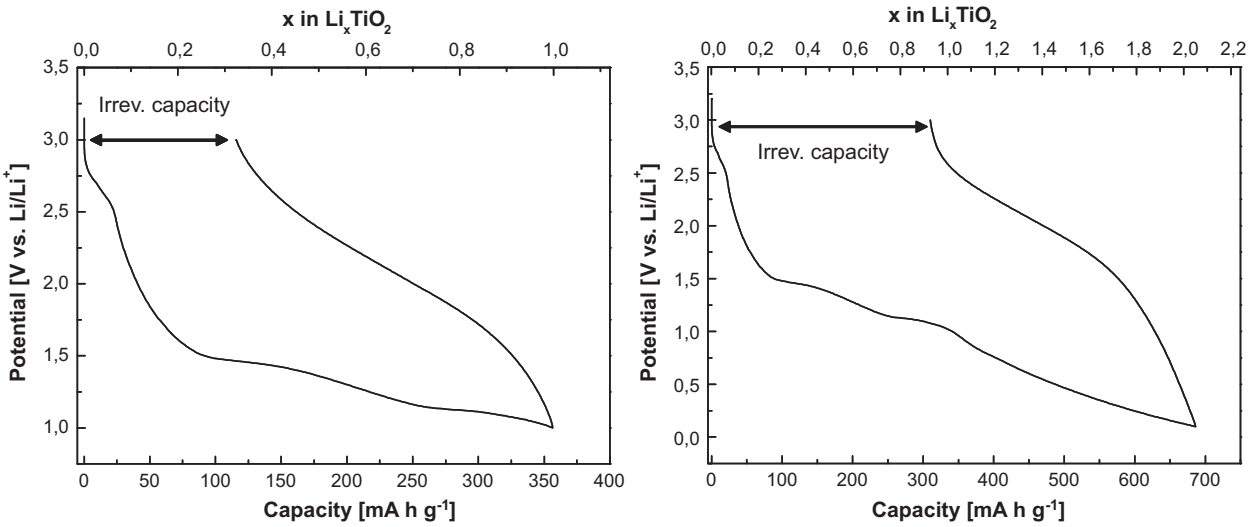

Fig. 5. Galvanostatic curves of the first discharge and charge in the potential window of 1–3 V (left) and 0.1–3 V (right). Arrows indicate the irreversible capacity loss in the first cycle.

graphite peak $A_{Gr.}$, we conclude that $A_{Rt.}$ is also related to a surface film (SEI) decomposition. The peak $A_{Rt.}$ was also present in a sample cycled between 1 and 3 V in the partly lithiated state (1 V) (Table 1) Therefore it is obvious that the SEI is also formed at potentials above 1 V but increases as we cycle down to 0.1 V. This additional SEI formation could be related to the peak at ~0.8 V in the cyclic voltammetry in our previous work [23]. The endothermic peak $B_{Rt.}'$ in the delithiated and in the partly lithiated (1 V) state (Table 1) is, like in the graphite electrode, related to the evaporation of the electrolyte. The nature of the exothermic peak $B_{Rt.}$ in the fully lithiated state (0.1 V) is up to now not understood and is under investigation in our lab. Additionally no oxygen release, which could lead to a sever safety problem, could be detected for rutile electrodes at any temperature. The thermal behaviour of delithiated rutile is, akin to graphite, endothermic and had one exothermic reaction related to the SEI decomposition. But the crucial point for of an anode material is the thermal stability in the lithiated state. At this point, the rutile sample appeared to be a very safe electrode material for lithium-ion batteries.

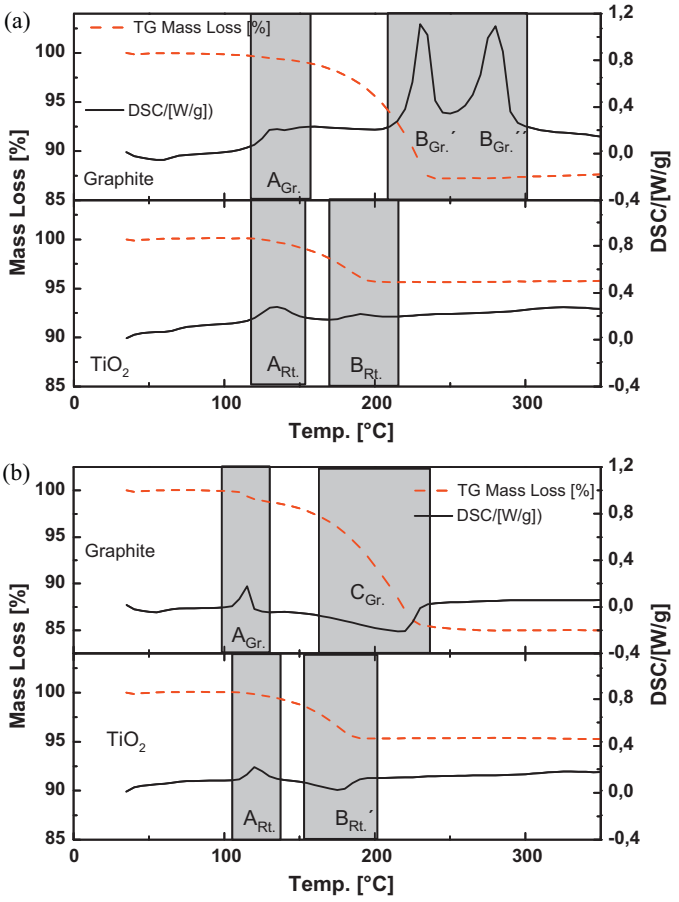

Fig. 6. DSC/TG curves of the (a) lithiated graphite (top) and rutile (bottom) electrodes and the (b) delithiated graphite (top) and rutile (bottom). Positive peaks are exothermic and negative ones endothermic.

3.3. Impedance measurements

To examine the nature of the irreversible capacity we performed impedance measurements at certain potentials in two potential windows, 1–3 V and 0.1–3 V, in the frequency range of 0.01–75,000 Hz. The shape of all diagrams showed one semicircle with a following diffusion region for both potential windows (Fig. 7a–d). A deeper insight into the spectra could be achieved using Boukamp and simulating the recorded data with an equivalent circuit. Two equivalent circuits (1, 2) were used to simulate the impedance spectra.

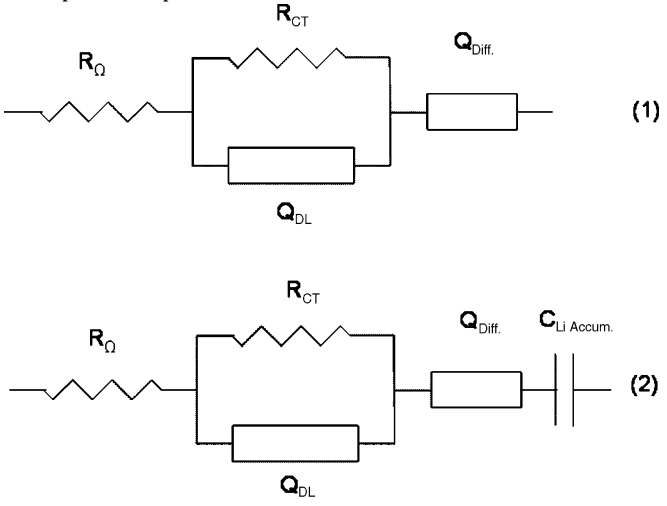

Table 1
Onset temperature and heat generation of the peaks in the DSC curve rutile (top) and graphite electrodes (bottom). Positive (+) ΔH values are exothermic and negative (−) ones are endothermic.

	$A_{Rt.}$		$B_{Rt.}$		$B_{Rt.}'$	
	Onset (°C)	ΔH (J g^{-1})	Onset (°C)	ΔH (J g^{-1})	Onset (°C)	ΔH (J g^{-1})
Rutile electrodes						
Delithiated (3.0 V)	112	8.7	152	−13.3		
Lithiated (1 V)	115	14.0	145	−10.9		
Lithiated (0.1 V)	118	18.3			178	3.0
	$A_{Gr.}$		$B_{Gr.}$		$B_{Gr.}' + B_{Gr.}''$	
	Onset (°C)	ΔH (J g^{-1})	Onset (°C)	ΔH (J g^{-1})	Onset (°C)	ΔH (J g^{-1})
Graphite electrodes						
Delithiated (1.5 V)	110	13.8	160	−67.4		
Lithiated (0.02 V)	120	27.3			223, 268	202.5

−, endotherm; +, exotherm.

An ohmic resistance (R_Ω) was used to describe the resistance of the electrolyte and cell components. A parallel circuit of a constant phase element and a resistance was taken for the double layer capacitance (Q_{DL}) and the charge transfer resistance (R_{CT}). Another constant phase element was used for the solid state diffusion of Li^+ ($Q_{Diff.}$). Impedance spectra below 1.5 V in the first discharge additionally showed a lithium accumulation at low frequencies represented by a capacitor ($C_{Li\ Accum.}$). Detailed results for the first cycle are given in Table 2.

In both potential windows 1–3 V and 0.1–3 V the ohmic resistance was comparable ~3 Ω and remained constant within the margin of errors. With higher Li^+ content in the discharge of TiO_2 we observed in both potential windows a higher charge transfer resistance. In the following charging cycle the two potential windows showed a completely different picture. In the 1–3 V region we observed a small increase (1.5 V) followed by a decrease of the charge transfer in the following cycle, while in the 0.1–3 V window the charge transfer was stable for the complete charge and all following impedance measurements. In the diffusion region at low frequencies (<10 Hz) we observed a Warburg like diffusion with $n_{Diff.}$ values (exponent of $Q_{Diff.}$) between 0.58 and 0.42 except for the beginning of the first discharge (2 and 1.5 V). The DSC/TA strongly indicates the formation of a SEI, thus we suggest that the SEI was present in the impedance measurements but the time constants

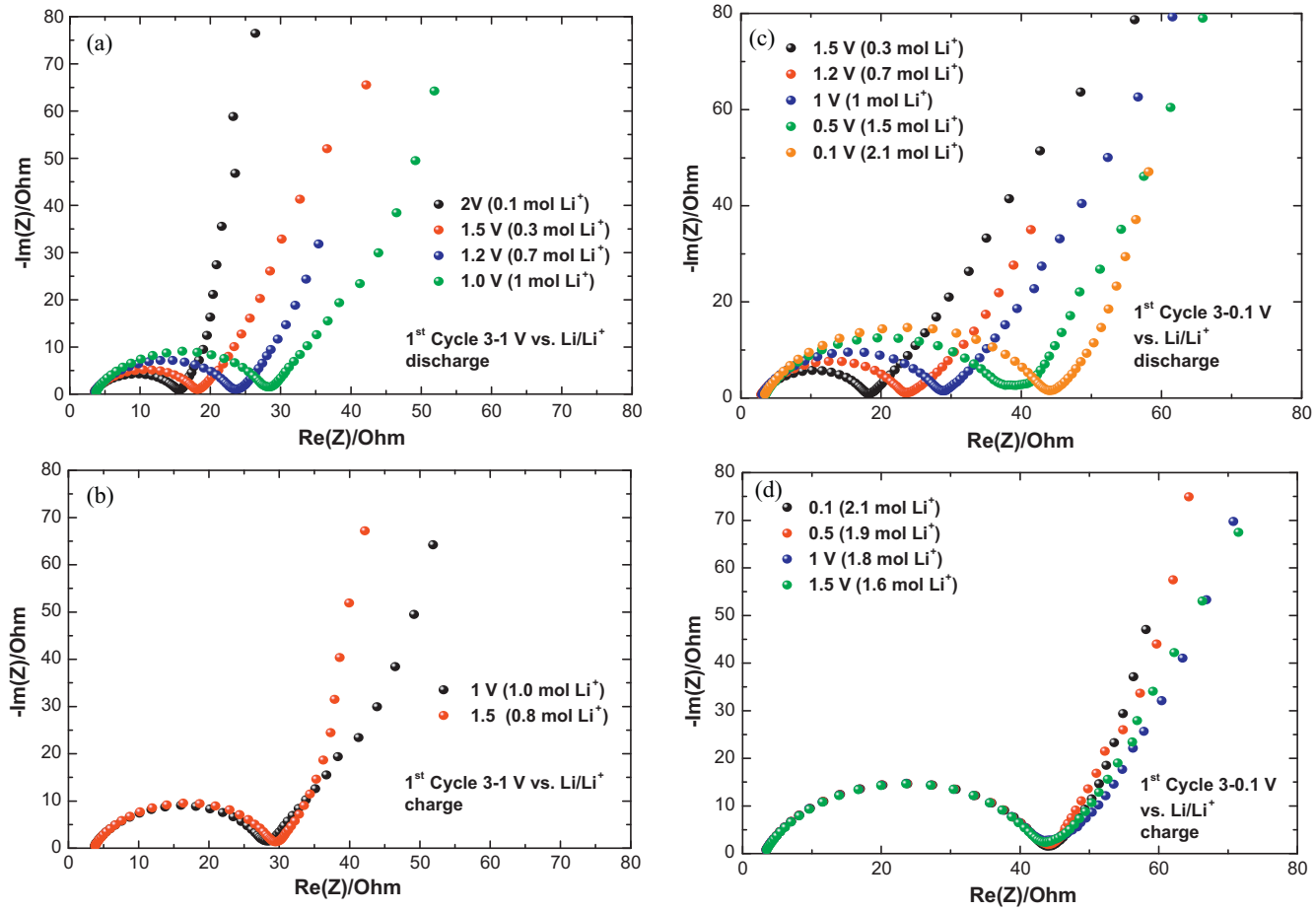

Fig. 7. Impedance spectra of the evaluated rutile samples: (a) 1st cycle discharge in the potential range of 3–1 V, (b) 1st cycle charge 1–3 V, (c) 1st cycle discharge 3–0.1 V, and (d) 1st cycle charge 0.1–3 V.

Table 2
Simulated values of the ohmic resistance (R_Ω), the charge transfer resistance (R_{CT}) and the exponent of the constant phase element of the diffusion ($n_{Diff.}$) in the 1st cycle (top) and second cycle (bottom).

	0.1–3 V			1–3 V		
	R_Ω	R_{CT}	$n_{Diff.}$	R_Ω	R_{CT}	$n_{Diff.}$
1st cycle						
Discharge						
2				3.3	12.8	0.89
1.5	2.7	15.8	0.7	3.3	15.2	0.77
1.2	2.7	20.4	0.48	3.4	19.8	0.48
1.0	2.8	25.6	0.42	3.6	24.5	0.58
0.5	3.2	34.7	0.50			
0.1	3.2	40.3	0.48			
Charge						
0.5	3.1	40.3	0.52			
1.0	3.1	39.3	0.42	3.6	24.5	0.58
1.5	3.2	39.9	0.52	3.6	25.5	0.5
2nd cycle						
Discharge						
2				3.7	21.2	0.52
1.5	3.3	41.8	0.45	3.6	23.7	0.53
1.2	3.3	42.0	0.49	3.6	25.5	0.45
1.0	3.2	41.3	0.42	3.7	27.2	0.51
0.5	3.1	42.6	0.52			
0.1	3.1	42.7	0.55			
Charge						
0.5	3.2	42.1	0.49			
1.0	3.3	41.2	0.42	3.7	27.2	0.51
1.5	3.4	41.8	0.53	3.8	28.2	0.49

for SEI and charge transfer were the same. Therefore it was not possible to resolve the two semicircles in the spectra. A strong indication of a stable SEI is the increasing semicircle in the discharge down to 0.1 V which remains constant in the following charge and discharge. In the potential window of 1–3 V the increasing semicircle in the discharge and the decreasing in the charge could be caused by a more dynamic film which was formed in the discharge and partially dissolved in the charge. To resolve the two semicircles further impedance studies at low temperatures are needed. Additional XPS analysis could identify the properties of the solid electrolyte interface.

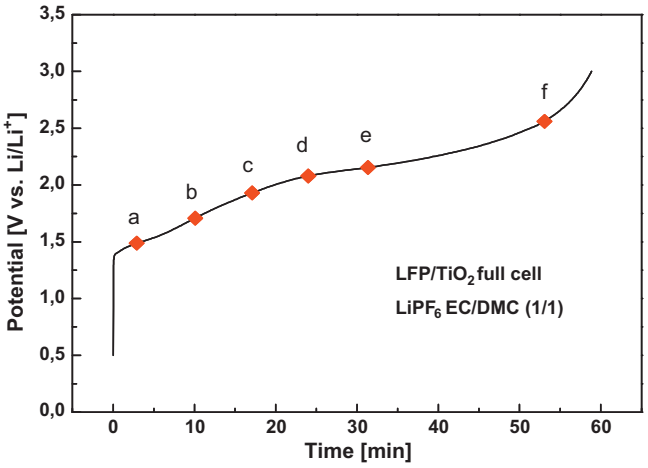

Fig. 8. Galvanostatic charge curve of the LFP/TiO_2 full cell (pouch), (♦) mark the selected in situ microscopy images. (For interpretation of the references to color in this figure legend, the reader is referred to the web version of this article.)

3.4. Pouch cell for in situ analysis

A new pouch cell design suitable for various in situ techniques is presented in Fig. 1a and b. In our case we performed in situ optical microscopy on a carbon free rutile electrode with a $LiFePO_4$ counter electrode. The hole in the middle of the cell enables a direct view on one electrode which is in our case the rutile anode. Upon lithium insertion into TiO_2 rutile (Fig. 8) the reduction of Ti^{4+} to Ti^{3+} occurs and is identified by a color change from beige to black (Fig. 9a–f). Once a black spot is formed, indicating an electronic change, a growth of other spots around the first one can be seen. After the rutile electrode had almost turned completely into black at ~0.5 mol Li^+ per mol Ti the color remains upon further lithiation and delithiation. This indicates that not all the Ti^{3+} formed during Li insertion is re-oxidized to Ti^{4+} upon delithiation. Further in situ measurements of the cycled Li_xTiO_y species are in progress in our lab to identify the reaction mechanism. The pouch cell was

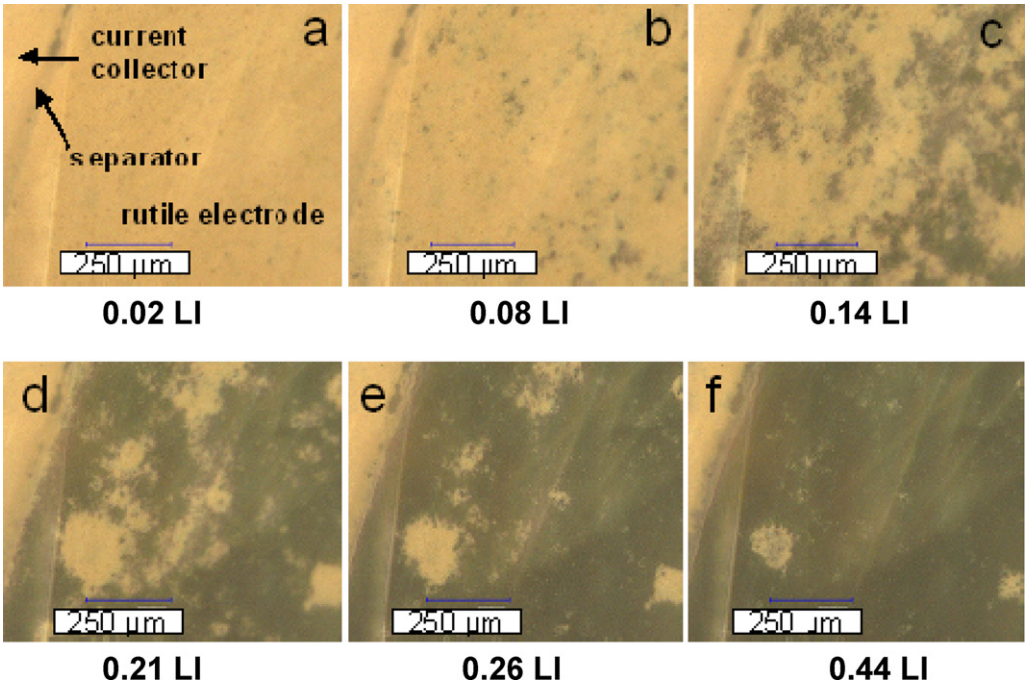

Fig. 9. Different in situ microscopy images of the hole in the pouch cell, recorded at different lithiation states (a–f) calculated for the rutile anode.

charged and discharged for several cycles without any problems of short circuits or lithium dendrite formation although no separator is covering the hole area of the rutile anode. Secondly the inhomogeneous current distribution does not lead to any electrochemical problems. Therefore this pouch cell design is very promising and allows the use of several in situ techniques (FTIR, Raman, XRD) to identify the material properties of a target electrode.

4. Conclusion

The nanosized rutile has, due to its small crystallite size and morphology, excellent electrochemical properties e.g. high capacity, high rate cycling up to 30 C and good capacity retention for fast cycling (1000 cycles at 5 C). TG/DSC measurements of lithiated and delithiated rutile showed only a small heat generation mainly related to a surface film decomposition (SEI), while graphite revealed strong exothermic reactions in the lithiated state. These findings proved the safer character of rutile electrodes in comparison to graphite. Impedance measurements showed only one semicircle in the spectra which was related to the charge transfer. It is suggested that the SEI was present in the impedance measurements but the time constants for SEI and charge transfer were the same. A strong indication of a SEI contribution is the increasing semicircle in the first discharge down to 0.1 V which remains constant upon further charge and discharge. In order to resolve the two semicircles further impedance measurements at low temperature are needed. A new pouch cell design which is suitable for in situ measurements was presented. With a hole in counter electrode ($LiFePO_4$) and in the separator we could directly view onto the target electrode. This lithium-ion full cell can provide useful information about the insertion mechanism and the ageing of the battery material and its functionality was demonstrated by in situ optical microscopy.

Acknowledgements

Financial support from BMBF in the framework of the LISA project (03SF0327A) and from Deutsche Forschungsgemeinschaft (DFG) within the Priority Program (SPP 1181) is gratefully acknowledged. The authors thank Prof. N. Hüsing and Dr. J. Geserick, Ulm University, Institute of Inorganic Chemistry I, for the synthesis of the rutile TiO_2, Dr. U. Hörmann and Prof. U. Kaiser from the University of Ulm, Electron Microscopy Group of Material Science for the TEM measurement and R. Stern and M. Wilka from Zentrum für Sonnenenergie- und Wasserstoff- Forschung for the pouch cell preparation.

References

[1] J.M. Tarascon, M. Armand, Nature 414 (2001) 359.
[2] P.G. Bruce, Solid State Ionics 179 (2008) 752.
[3] A.S. Arico, P. Bruce, B. Scrosati, J.M. Tarascon, W. Van Schalkwijk, Nat. Mater. 4 (2005) 366.
[4] C.-K. Huang, J.S. Sakamoto, J. Wolfenstine, S. Surampudi, J. Electrochem. Soc. 147 (2000) 2893.
[5] R. Fong, U. von Sacken, J.R. Dahn, J. Electrochem. Soc. 137 (1990) 2009.
[6] E.P. Roth, D.H. Doughty, J. Power Sources 128 (2004) 308.
[7] H.H. Lee, C.C. Wan, Y.Y. Wang, J. Electrochem. Soc. 151 (2004) A542.
[8] H. Yang, H. Bang, K. Amine, J. Prakash, J. Electrochem. Soc. 152 (2005) A73.
[9] Q. Wang, J. Sun, X. Yao, C. Chen, J. Electrochem. Soc. 153 (2006) A329.
[10] B. Zachau-Christiansen, K. West, T. Jacobsen, S. Atlung, Solid State Ionics 28–30 (1988) 1176.
[11] D. Murphy, R. Cava, S. Zahurak, A. Santoro, Solid State Ionics 9–10 (1983) 413.
[12] Z. Yang, D. Choi, S. Kerisit, K.M. Rosso, D. Wang, J. Zhang, G. Graff, J. Liu, J. Power Sources 192 (2009) 588.
[13] L. Kavan, M. Grätzel, J. Rathousky, A. Zukal, J. Electrochem. Soc. 143 (1996) 394.
[14] W.J. Macklin, R.J. Neat, Solid State Ionics 53 (1992) 694.
[15] Y.S. Hu, L. Kienle, Y.G. Guo, J. Maier, Adv. Mater. 18 (2006) 1421.
[16] M.A. Reddy, M.S. Kishore, V. Pralong, V. Caignaert, U.V. Varadaraju, B. Raveau, Electrochem. Commun. 8 (2006) 1299.
[17] E. Baudrin, S. Cassaignon, M. Koesch, J.P. Jolivet, L. Dupont, J.M. Tarascon, Electrochem. Commun. 9 (2007) 337.
[18] S. Bach, J.P. Pereira-Ramos, P. Willman, Electrochim. Acta 55 (2010) 4952.
[19] M.V. Koudriachova, N.M. Harrison, S.W. de Leeuw, Phys. Rev. Lett. 86 (2001) 1275.
[20] M.V. Koudriachova, N.M. Harrison, S.W. de Leeuw, Solid State Ionics 35 (2003) 157.
[21] O.W. Johnson, Phys. Rev. 136 (1964) A284.
[22] F. Gligor, S.W. de Leeuw, Solid State Ionics 177 (2006) 2741.
[23] M. Pfanzelt, P. Kubiak, M. Wohlfahrt-Mehrens, Electrochem. Solid State Lett. 13 (2010) A91.
[24] P. Kubiak, M. Pfanzelt, J. Geserick, U. Hörmann, N. Hüsing, U. Kaiser, M. Wohlfahrt-Mehrens, J. Power Sources 194 (2009) 1099.
[25] B.A. Boukamp, Solid State Ionics 18–19 (1986) 136.
[26] B.A. Boukamp, Solid State Ionics 20 (1986) 31.